

## **Fracture of mobile unicompartmental knee bearings: a parametric finite element study**

Elise C. Pegg<sup>1\*</sup>, David W. Murray<sup>1</sup>, Hemant G. Pandit<sup>1</sup>, John J. O'Connor<sup>3</sup>, Harinderjit S. Gill<sup>2</sup>

<sup>1</sup> Nuffield Department of Orthopaedics, Rheumatology and Musculoskeletal Sciences, University of Oxford, Oxford, OX3 7LD.

<sup>3</sup> Department of Engineering Science, University of Oxford, OX1 3PJ.

<sup>2</sup> Department of Mechanical Engineering, University of Bath, Claverton Down, Bath, BA2 7AY

\*Corresponding Author:

Elise C Pegg, PhD

Address: University of Oxford

Nuffield Department of Orthopaedics, Rheumatology and Musculoskeletal Sciences,  
Nuffield Orthopaedic Centre,  
Windmill Road,  
Oxford, OX3 7LD.

Email: [elise.pegg@ndorms.ox.ac.uk](mailto:elise.pegg@ndorms.ox.ac.uk)

Fax: +44 (0) 1865 227671

Tel: +44 (0) 1865 227663

Running title: Fracture of unicompartmental knee bearings

## **Abstract**

Cases of fractured mobile unicompartmental knee bearings have recently been reported, the purpose of this study was to understand the mechanics behind these fractures and to examine the influence of different design modifications. A parametric finite element model was used to examine the influence of different geometrical factors on the stresses within the bearing. Crack initiation occurred clinically in the centre of the bearing, this correlated with the position of the maximum von Mises stress. Tensile stresses, thought to propagate the fatigue crack, were maximal at the medial-lateral sides of the bearing, and the tensile vectors were normal to the fracture direction observed clinically. Fully congruent femoral articulation on the bearing, use of a thicker bearing size, and minimising wear of the component; all reduced the risk of fracture. For example, an unworn 6.5 mm thick bearing (no clinical fractures reported) had 21.6% lower medial-lateral tensile stress compared to an unworn 3.5 mm bearing (5 clinical fractures reported). In turn, an unworn 3.5 mm bearing had 34.3% lower tensile stress compared to a 3.5 mm bearing after 1.9 mm wear (average linear wear reported for clinically fractured bearings). The fracture risk was also reduced when the radio-opaque marker wire was positioned further from the centre of the bearing, and when marker balls were used instead of marker wires (19% reduction in some regions). These results indicate the importance of minimising component wear; the data also supports the current component design which uses posterior marker balls instead of marker wires, and the continuing use of a congruous femoral component.

Keywords: knee replacement, polyethylene, fracture mechanism, finite element analysis, stress analysis, crack.

## Introduction

Fracture, whilst rare, is a concern when using mobile bearings in unicompartmental knee replacement. With increasing usage of these components [1] and longer life expectancy [2], it is essential to reduce the risk of fractures occurring. In a recent study, ten retrieved Oxford Unicompartmental Knee Replacement (UKR) (Biomet UK Healthcare Ltd., Swindon, UK) ultra-high molecular weight polyethylene (UHMWPE) bearings were examined that had fractured during use [3]. The average time *in situ* prior to fracture was 16.8 years and the incidence of fracture was 3.2% for the Phase 1 (used prior to 1987), 0.74% for Phase 2 (used prior to 1998) and 0.35% for Phase 3 bearings manufactured prior to 1999. However, the more recent designs have not been in general use for as long and so the range of follow-up time is reduced. From 1999 onwards, the bearing for the Oxford UKR uses two marker balls instead of a posterior marker wire (Figure 1); no fractures of the bearings with marker balls have been reported. The purpose of the marker is to aid location of the bearing on a radiograph of the knee, because polyethylene is not radio-opaque.

In the previous retrieval study, the fracture surface patterns indicated that the failures had occurred due to fatigue fracture, and that the cracks were initiated in the centre, at the thinnest part of the bearing. The direction of the fractures was comparable in eight of the ten bearings, in these cases there was a single fracture which was in the medial-lateral (ML) direction. The bearings showed evidence of impingement, above average wear, and oxidation. In addition to this, four of those eight fractures went through or were near to the posterior radio-opaque marker wire; thus it is probable that the wire was an influencing factor for some of the fractures.

Increased *in vivo* wear rates have been linked with impingement of the UHMWPE bearing on the surrounding bone or cement [4, 5], this wear can lead to weakening and an increased risk of fracture [6]. Impingement and high wear was evident in all the fractured bearings and is thought to play a major role in the mechanism of fracture [3]. The quality of the UHMWPE used to manufacture a component is also thought to have been a factor [3, 7].

However, the inconsistent quality of the early generation UHMWPE, and excessive wear due to impingement, does not answer all of the questions raised by the previous study. The mechanism by which the radio-opaque marker wire, and its position, influences the fracture risk is unknown. The importance of other geometrical factors, such as bearing thickness or femoral congruency, is also undetermined. In addition, the reason why the fractures occur, in general, in the ML direction is currently unconfirmed; although the previous study suggested this may be due to tensile forces resulting from the outward force component of the spherical articular pressure [3].

The purpose of this study was, firstly, to test the hypothesis that tensile forces within the bearings caused the characteristic ML fracture direction; and secondly, to investigate the influence of various design parameters on the risk of fracture of Oxford UKR bearings.

## **Materials and Methods**

### *Parametric bearing model*

The geometry of the bearing model was based upon the Phase 1 design of the Oxford UKR, as the highest incidence of fracture was found with this design [3]. The Phase 1 femoral design was available in only one size (spherical radius of 24 mm); but the bearing came in a variety of thicknesses, ranging from 3.5

mm at the bottom of the spherical concavity, to 11.5 mm, in steps of 1 mm. The design was symmetric in the anterior-posterior plane and therefore it was only necessary to model half of the bearing.

Parametric models were created to enable factors to be examined individually. Python (version 2.6, Python Software Foundation, NH, USA) was used to write the scripts which created the models within the FEA software. All simulations were performed using ABAQUS FEA software (version 6.11, Simulia, Rhode-Island, USA). Geometrical models investigated included; varying the position of the marker wires/balls in the  $y$ -direction ( $m_1$ ), the femoral radius ( $f$ ), the bearing thickness ( $t$ ), and the backside wear; the marker height ( $m_2$ ) in relation to the spherical surface was kept constant (Figure 2, Table 1). Backside wear was modelled as a reduction in bearing thickness while keeping the marker in the same position. ( $t-m_2 = 0.5$  mm).

Two main models were examined; bearings with marker wires (Model W), and those with marker balls (Model B) (Figure 2a). The holes for the marker wire went through the entire width of the bearing, the holes for the marker balls went to a depth of 3 mm from the outer surface. The default dimensions used for the models ( $t = 3.5$  mm,  $f = 24$  mm,  $m_1 = 10.5$  mm,  $m_2 = 3$  mm, Figure 2b) were taken from product documentation where possible; and in cases where the values were unknown, direct measurements were made on components. The femoral component was positioned concentrically onto the spherical upper surface of the bearing so that the two lowest points of the spheres were in contact.

#### *Material properties*

A quasi-static finite element model with an explicit direct solver was used for all simulations; it was therefore necessary to include specification of the mass (or density), as well as the modulus and Poisson's ratio, of all materials. The femoral component and the marker wires/balls were modelled as analytical

rigid surfaces. The UHMWPE bearing was modelled assuming isotropic  $J_2$  plasticity (simple elastic-plastic response); with a Poisson's ratio of 0.46 [8], a density of  $0.95 \text{ g/cm}^3$  (representing irradiated UHMWPE aged *in vivo* by 5 years [9, 10]) and a Young's modulus of 315 MPa and a yield stress of 11 MPa. The plasticity data used was taken from the work by Bergstrom *et al.* and was calculated from the true half-cycle stress-strain data for UHMPWE after reaching cyclic stability [11].

The mass assigned to the femoral component (half model) was 17.1 g, this was calculated from a Cobalt Chromium Molybdenum alloy density of  $8.387 \text{ g cm}^{-3}$  [12] and a femur volume of  $2.04 \text{ cm}^3$ . The mass assigned to the marker wires was 0.419 g and the marker balls was 0.00863 g; this was calculated using a volume of  $0.00942 \text{ cm}^3$  for the marker wire, using a Titanium 6-Aluminium 4-Vanadium alloy density of  $4.42 \text{ g cm}^{-3}$  [13], and  $0.00052 \text{ cm}^3$  for the marker ball, using a Tantalum density of  $16.6 \text{ g cm}^{-3}$  [14].

#### *Boundary conditions*

The base of the bearing was constrained in the  $z$ -axis, and the femoral component was only permitted to translate in the  $z$ -axis. Symmetric constraints were applied to the end of the marker wires in the  $x$ -axis and the markers were also prevented from rotating (Figure 3). A friction coefficient of 0.07 [15] was used for contact (penalty algorithm) between the femoral component and the bearing, and the marker wire/ball and the bearing. Articulation of the tibial side of the bearing was assumed to be frictionless.

A sinusoidal cyclic load was applied to the femoral component to a maximum of 2.4 kN, at a frequency of 1 Hz. The load value used was based on a patient of weight of 80.1 kg, which was the average reported patient weight of the cases of clinical fractures [3], during walking (3 times body weight [16]). To ensure efficient model run-time, a mass-scaling factor of  $4 \times 10^5$  was used [17].

### *Mesh definition*

The bearing was meshed using quadratic tetrahedral elements (C3D10). Seeding of the mesh was performed in two stages. Firstly, the whole bearing was seeded using a set overall mesh size. Secondly, certain regions in the model were seeded with a further refined mesh size, which was 30% of the overall mesh size. The refined mesh regions were; the ML sides of the bearing, the marker holes, and the region in the centre. Once seeded, the model was meshed using the automatic mesh creation tools within ABAQUS. A mesh convergence test, with element sizes ranging from 2.8 mm to 0.5 mm (Table 2), found an overall mesh size of 1 mm to be optimum; where the result was within 95% of the next three smaller mesh sizes (Figure 4). The final model had 59,167 nodes and 39,870 elements.

### *Statistics*

A probabilistic approach was used to analyse the results from the study statistically, the method used was that detailed by Dar *et al.* [18]. The same model was run 40 times, but each time a random error was added to the geometrical dimensions of the component, the possible error range was based upon manufacturing tolerances. Thus 40 models were created for one specific bearing, which should represent the variation seen in the dimensions of 40 manufactured components. The variation in the finite element analysis results from these models was then used for statistical analysis when comparing whether there was a statistical significance between two results.

The dimensions to which tolerance variation was applied were; the femoral radius, the bearing thickness, the marker position, the femoral width, the bearing width and length, and the marker hole diameter. The tolerance value used for the marker hole was  $\pm 0.02$  mm, which was based upon standard specifications (ISO 286-2: 2010, Geometrical product specifications (GPS)); and for all other dimensions a tolerance of  $\pm 0.1$  mm was used, equivalent to an average CNC machine cutting tolerance. A random number

generator ('random' module within Python) with a Gaussian distribution within the tolerance values was used to add error to each dimension.

Statistical tests were performed to compare differences between the models tested; when considering only two sets, a Student's *t*-test was performed, and for all other tests one-way analysis of variance (ANOVA) with a Tukey post-hoc test was used. The Pearson's correlation coefficient and coefficient of determination ( $R^2$ ) were found when performing linear regressions between factors.

#### *Model validation*

Firstly, to ensure that the mass-scaling factor did not affect the results, the kinetic energy of the model (default dimensions) was compared to the internal energy [19]. The kinetic energy was 0.02% of the internal energy of the model and therefore was deemed acceptable. In addition to this, an equivalent implicit model was created and the results compared to that of the quasi-static model, no significant difference was found in the stresses within the bearing.

Secondly, to assess the importance of modelling the friction on the tibial side of the bearing, two models were created and compared; one with and one without friction. A flat analytical rigid surface was used to model the tibial tray, and a friction of 0.07 [15] was defined for the articulation of the bearing on the tray; all other parameters were the same as the 'default' bearing model. The results found the friction caused a 6.8% reduction in the tensile stress range at the side of the bearing, a 7.6% reduction within the marker hole and a 0.2% increase in the von Mises stress (Figure 5). None of these changes in stress were found to be significant.



Thirdly, the results of the finite element model were compared to experimental measurements. A 5.5 mm thick bearing sample (Biomet UK Ltd., Swindon, UK) was loaded 20 times sinusoidally between 0.24 kN and 2.4 kN at a frequency of 1 Hz using a servo-hydraulic test machine (Dartec HC10, Zwick Testing Machines Ltd., Leominster, UK) with a calibrated 15 kN load cell. A resistance-based 28 mm by 33 mm pressure sensor with 572 sensels (Model 4000, Tekscan, Boston, USA) was placed underneath the bearing during loading, the surface of the sensor was coated in lubricant to minimize shear forces.

The sensor was conditioned prior to loading, using the method detailed by Brimacombe et al. [20], which involved four cycles. Each conditioning cycle started with a linear increase in load over 10 s, the load was then held constant for 5 seconds, followed by a linear decrease for 10 s and the sensor was then left unloaded for 120 seconds before the next cycle. The sensor was then equilibrated, and then calibration was performed by loading to 10 different random loads between 10% and 100% of the estimated load. The applied loads and resultant forces on the sensor were calibrated using a power law. The maximum pressure under the bearing predicted by the finite element model was  $8.3 \pm 1.60$  MPa, which was within 9.8% of the  $9.21 \pm 0.39$  MPa measured by the pressure sensor. When the variation in the models was taken into account, no statistical difference was found between the datasets ( $p=0.1066$ ).

## Results

At the peak load of the first loading cycle, the maximum von Mises stress was in the centre of the bearing at the base and was above the yield stress of the material. A high tensile stress range (difference between the peak tensile stress and residual stress after unloading) was found within the marker wire hole and was also evident along the side of the bearing (Figure 6). At the side of the bearing the direction of the tensile stress (represented by red arrows in Figure 7) was normal to the ML plane, running in the anterior-

posteriorly. The maximum net total force acting on the ML plane in the centre of the bearing was tensile, and was of a magnitude of 130 N (5.4% of total load, Figure 8), irrespective of thickness.

Upon subsequent loading cycles, a slight drop in stress (2% for von Mises stress, 13% for the tensile stress) was observed for the second loading cycle; this drop was significant for the von Mises stress ( $p=0.0310$ ), and for the tensile stress ( $p<0.0001$ ). Thereafter, no significant changes ( $p>0.8700$ ) in stress were observed (Figure 9). A reduction of 1.7% was also found in the net total tensile force on the fracture surface (Figure 8).

The tensile stress within the posterior marker hole within the bearing was, on average, 52.9% higher than in the anterior marker hole; this difference was significant ( $p<0.0001$ ). Replacement of the posterior radio-opaque marker wire with marker balls had the greatest effect on the tensile stresses within the marker hole, these were significantly ( $p=0.0294$ ) reduced by 18.7% on average (Figure 10c). A reduction was also seen at peak loading in the tensile stresses at the side of the bearing (average 3.5% reduction,  $p=0.0110$ , Figure 10b). No significant change was found in the von Mises stress at the centre of the bearing ( $p=0.1327$ , Figure 10a).

Placement of the marker wire towards the centre of the bearing caused a proportional increase in the tensile stress within the marker hole ( $R^2=0.788$ ,  $p=0.0033$ , Figure 10c), the stress increased at a rate of 0.788 MPa / mm from the centre. An increase in tensile stress was also found during peak loading at the side of the bearing (Figure 10b); however, it was only at a magnitude of 0.0046 MPa / mm ( $R^2=0.8370$ ,  $p=0.0014$ ) and the von Mises stress in the centre of the bearing increased at a rate of 0.0164 MPa / mm ( $R^2=0.6870$ ,  $p=0.0109$ , Figure 10a).

Backside wear of the bearing caused a proportional increase in tensile stresses at the side (0.859 MPa/mm,  $R^2=0.9980$ ,  $p<0.0001$ , Figure 10b) and the von Mises stress at the centre (1.59 MPa/mm,  $R^2=0.9700$ ,  $p<0.0001$ , Figure 10a) during peak loading. When the bearing was worn by 1.9 mm, the peak stresses at the side increased by 37.1%, and by 29.6% in the centre of the bearing.

All the stress within the bearing evaluated in this study significantly increased as the spherical radius of the femoral component was reduced (Figures 10a-c), but not linearly; the rate of increase reduced with decreasing radii. The maximum von Mises stress and the tensile stress range at the side of the bearing increased significantly at each reduction (average  $p<0.0001$  for von Mises stress, average  $p<0.0001$  for tensile stress). The tensile stress within the marker hole became significantly increased by a femoral radius of 20.4 mm and above ( $p=0.0007$ ). By a femoral radius of 15.6 mm the tensile stress during peak loading had increased by 168 %, the von Mises stress in the centre (peak load) by 63 % and within the marker hole by 24.6 %.

The thinner bearings had greater stresses compared to the thicker bearing sizes (Figures 10a-c). Each 1 mm increase in thickness led to a significant reduction in the maximum von Mises stress ( $p<0.0010$ ) and a significant reduction in the tensile stress at the side of the bearing was found up until a thickness of 6.5 mm ( $p<0.0010$ ). A marked difference was observed in the tensile stress within the marker hole of the thinnest bearing (3.5 mm thick) compared with the other bearing sizes (43 % higher,  $p<0.0001$ ).

## **Discussion**

The main aims of the study were to; firstly, understand the fracture mechanism which resulted in the characteristic fracture pattern, and secondly, to examine the influence of various different design factors on the risk of fracture.

### *Fracture mechanism*

For a fatigue fracture to occur, first a crack needs to initiate or be already present within the material and develop into a micro-crack (Stage I), cyclic tensile forces of a sufficient tensile range are required to propagate the crack (Stage II), and finally the crack needs to reach a sufficient size before accelerating to catastrophic failure (Stage III) [21].

A previous SEM examination of a bearing fracture surface revealed fatigue striations on the fracture surface, which progressed outwards from the centre of the bearing [3]; this indicates that the Stage I crack occurred in the centre of the bearing. The results of the FEA demonstrated that the centre of the bearing was the site of the greatest von Mises stress (Figure 6), which was above the yield stress of the material. Studies have shown that cracks can initiate within UHMWPE when exposed to high compressive stress [22], and that cyclic damage of the UHMWPE and defect formation is most likely to occur in a region of plastic deformation [23]; it is therefore probable that the crack initiation occurred in the centre of the bearing due to high cyclic compressive stress.

Stage II crack growth in the retrieved bearings had occurred in the ML direction; it is known that Stage II crack growth occurs normal to the principal tensile axis [24, 25], and therefore it can be inferred that high tensile forces were present in the anterior-posterior direction. The FEA model confirmed this hypothesis, a net tensile force was acting on the fracture surface and represented approximately 5% of the total femoral load. The concentration of force was greatest at the medial and lateral sides of the bearing (Figure 7a) and therefore this region was used to assess risk of crack propagation.

### *Effect of multiple loading cycles*

Softening of the UHMWPE was observed when the bearing was loaded for multiple loading cycles, resulting in a slight drop in the stresses within the bearing and in the tensile forces on the fracture surface (Figure 9). A similar stabilisation was observed by Estupiñán *et al* [26] who also used a  $J_2$ -plasticity model and found no change in the results after 5 loading cycles of UHMWPE. Softening of UHMWPE has been demonstrated under experimental conditions and is a known phenomenon; however, it is thought that  $J_2$ -plasticity models over-estimate this effect [27]. A slight reduction in the net total tensile force acting on the fracture surface was also observed after multiple loading cycles (Figure 8); however, this difference was only 1.7% and implies that the force acting on the fracture surface would remain relatively stable throughout the lifetime of the component.

#### *Impact of the marker wire*

In four of the ten fractured bearings reported previously, the marker wire was implicated as a possible cause [3]. In these cases, the components were small bearings, which are known to have the marker wire closer to the centre; and the fracture was in the region of the posterior marker wire rather than the anterior wire. Movement of the marker wire closer to the centre of the bearing caused a linear and significant increase in all of the stresses within the bearing confirming that the position is important. The FEA results also found that the tensile stress in the region of the posterior marker wire is significantly greater than near the anterior marker wire. The posterior marker wire is in a thinner part of the bearing, the reason for this is that the anterior portion of the bearing was raised compared to the posterior to reduce the risk of posterior bearing dislocation and thus the thinnest part of the bearing became more posterior [28]. There is also anecdotal evidence that the backside wear of the bearing is greater posteriorly which would further exacerbate the stresses. The radio-opaque posterior marker wire was replaced with marker balls in 1999, the results from the present study indicate that this change has reduced the residual tensile stress within the marker hole by 53% and also caused a small reduction in tensile stress at the side of the

bearing. It is therefore likely that this has reduced the fracture risk, which is supported by the clinical evidence [3].

#### *Bearing wear*

General wear of the bearing is known to be an important factor, all of the bearings which fractured clinically had worn excessively and demonstrated evidence of impingement and oxidation [3]. Wear has been related to impingement [4, 5], and oxidation of UHMWPE has also been shown to increase wear and decrease fracture resistance [29]. Of the fractured bearings examined, the average linear wear was 1.9 mm [3]; according to the results, this amount of wear would cause a 30-40% increase in the stress within the bearing. Good surgical technique is therefore imperative to ensure that impingement does not occur, and storage of the component in accordance with the manufacturer's guidelines to avoid component oxidation is essential; these precautions should minimise wear and therefore to keep the stresses within the bearing at a low level.

#### *Femoral congruency*

The design philosophy behind the Oxford UKR is that the femoral component is fully congruent with the articulating surface of the bearing, and that the bearing is fully mobile on the flat tibial tray; the purpose of this is to minimise constraint while maximising contact area and minimising wear [4]. The models which loaded the bearing with a fully conforming femoral component demonstrated the lowest stresses, supporting the design philosophy. Unconforming mobile unicompartmental knee designs are in clinical use; some designs can have a high flexion geometry with a radius as low as 60-70% of the size of the congruent femur (measurements taken from product documentation images), equivalent to a 15.6 mm radius for the Oxford UKR. According to the results of this study, this non-congruency could cause an increase of 168% in stresses at the side of the bearing, 63% increase in stresses in the centre, 25%

increase in residual stresses in the centre of the bearing; all of which would be expected to increase the risk of fracture.

#### *Bearing thickness*

Of the ten fractured bearings examined, all were within the three smallest thicknesses (3.5 mm to 5.5 mm thick); however, it was not possible to conclude from the clinical data whether bearing thickness was a significant factor in the fractures due to the small number of clinical samples. The FEA results indicate that bearing thickness is an important factor in the fractures because the thinnest bearings had an increased von Mises stress and tensile stress range at the side of the bearing and within the marker hole. However, it is important to note that although these bearings have an increased risk of fracture, fracture of the bearings has only occurred clinically under oxidation, impingement, adverse wear conditions, and after a long period of time *in vivo*. The fractures appear to be a very time-dependent phenomenon; the average implantation time prior to fracture of the bearings was over 16 years, which would represent approximately 16,000,000 loading cycles; and some were implanted for over 20 years prior to fracture.

#### *Validity of the model*

There are limitations to the model used in this study; firstly, the  $J_2$ -plasticity material model used to represent the behaviour of UHMWPE was relatively simple, and is known not to be accurate for certain conditions. These include large deformations, rate-dependent behaviour, and for compressive strains above 0.6 [11, 30]. However, the  $J_2$ -plasticity model was thought to be appropriate for this particular study because the simulation did not involve large deformations, compressive strains did not exceed 0.6 and the rate used was constant and equal to both the material testing rate and the approximated *in vivo* loading rate. In addition to this, a small validation study using pressure sensors confirmed that the results from the finite element model were correct to within 10% of the measured values, which supported the

material model used. However, it is worth noting that the model does not take account of polyethylene creep which can occur over long periods of time. In addition, the model does not account for oxidation, which is known to increase exponentially with time *in vivo* [31], causing a reduction in the toughness [10], and an increase in modulus [32]. The model is only appropriate to simulate the behaviour of a newly manufactured bearing during the first few loading cycles.

Some assumptions were made in the model design. It was assumed that the articulation of the backside of the bearing with the metallic tray was frictionless and it is known that the friction coefficient between UHMWPE and cobalt-chrome-molybdenum alloy is approximately 0.07 [15]. No significant differences could be detected between the models run with, and without friction. The model assumed that the femoral loading was concentric to the bearing; however, in reality in some clinical cases abnormal loading conditions can cause eccentric articulation, and this was evident on some of the retrieved bearings [3]. Examination of this issue was outside of the scope of this study, but future work is underway to quantify the incidence, extent and influence of eccentric articulation.

Finally, it was evident that the variation in the results obtained from the region of the marker hole was greater than those in the centre of the bearing and the ML sides. This is thought to have been due to the contact definition in the region. Due to this variation, the model would have been unable to detect subtle changes in the results.

## **Conclusions**

Of the various geometrical parameters examined, the backside wear and the femoral incongruency increased the fracture risk the most. Based upon this, use of a non-congruent femur would not be



recommended and backside wear should be minimised. Wear is multifactorial, but impingement is known to be an important factor in cases of high wear in unicompartmental knee replacement [4, 5, 33] and therefore good surgical technique is paramount to reduce impingement. The use of thicker bearings was also shown to reduce the fracture risk; however, in practice the use of thicker knee bearings requires removal of more bone, and therefore should be carefully considered. Current evidence indicates that the use of the thinner bearings will only increase the risk of fracture when in combination with high wear, impingement, oxidation, and after a long time *in vivo*. Unfortunately it was not possible to account for *in vivo* aging of the polyethylene in this study but work is underway to examine the effect of these changes in the material properties. Other future work planned includes analysis of the common patterns of wear from retrieved specimens, and an investigation of the impact this might have on the stresses within the bearings. Finally, this study supports the design change made in 1999 where the posterior radio-opaque marker wire was replaced with two marker balls; the results indicate this will have significantly reduced the risk of bearing fracture.

### **Acknowledgements**

The authors would like to thank the University of Oxford for the departmental funding which was used to support this study, and also to Mr Alex Liddle for his invaluable help with the pressure sensor measurements.

### **Declaration of conflicting interests**

One or more of the authors have received payment from the manufacturer of the device examined in this work, however the funding was unrelated to this study and the manufacturer has had no influence on the information reported.

## Figure Captions and Tables

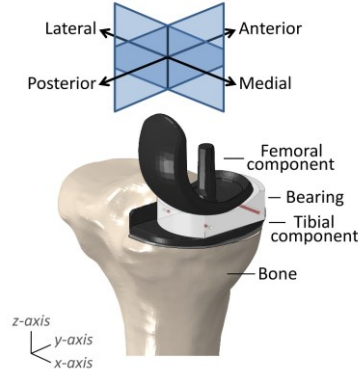


Figure 1. Position of the posterior marker balls and anterior marker wire (red) within the current bearing design. The components are shown implanted within the bone when the knee is in a standing position.

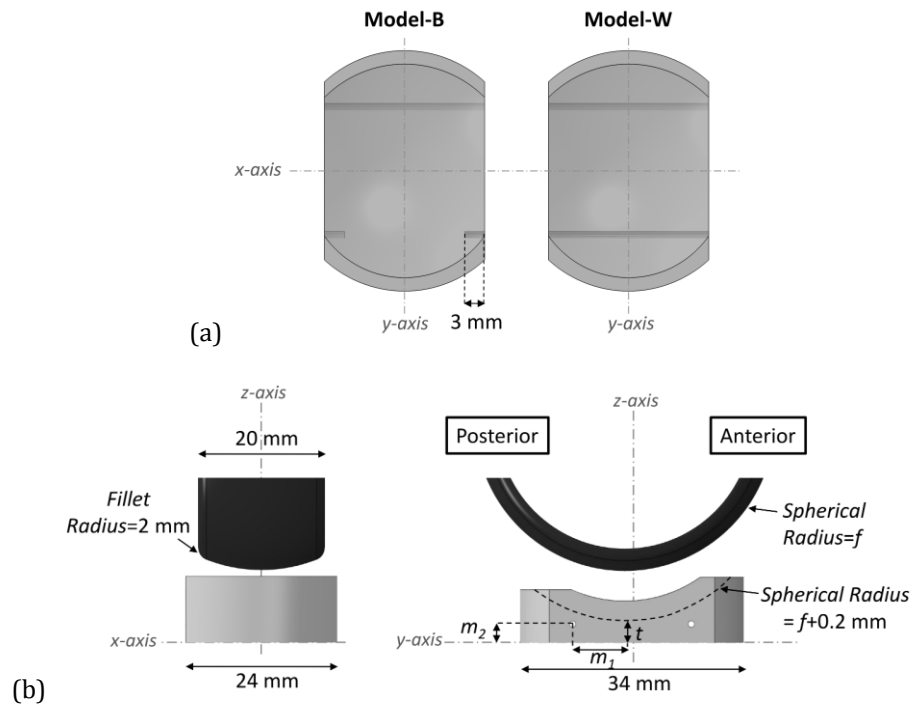


Figure 2. Illustration of (a) Model-W and Model-B geometry, and (b) the dimensions used to create the parametric model. Where,  $m_1$  = marker position in the  $y$ -axis,  $m_2$  = marker position in the  $z$ -axis,  $t$  = bearing thickness, and  $f$  = femoral spherical radius.

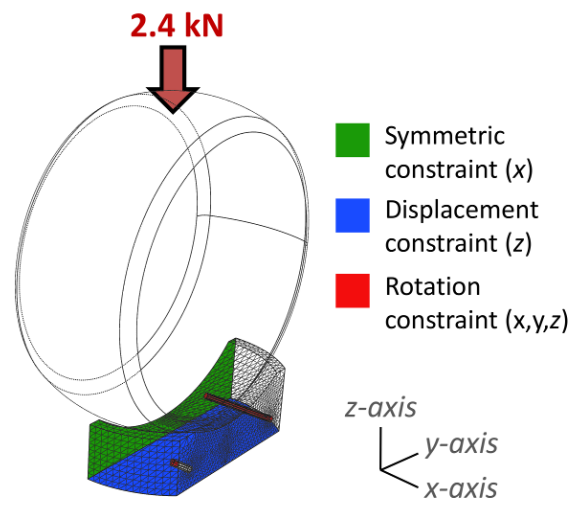


Figure 3. Illustration of the final mesh (1 mm overall size) and boundary conditions applied to the model.

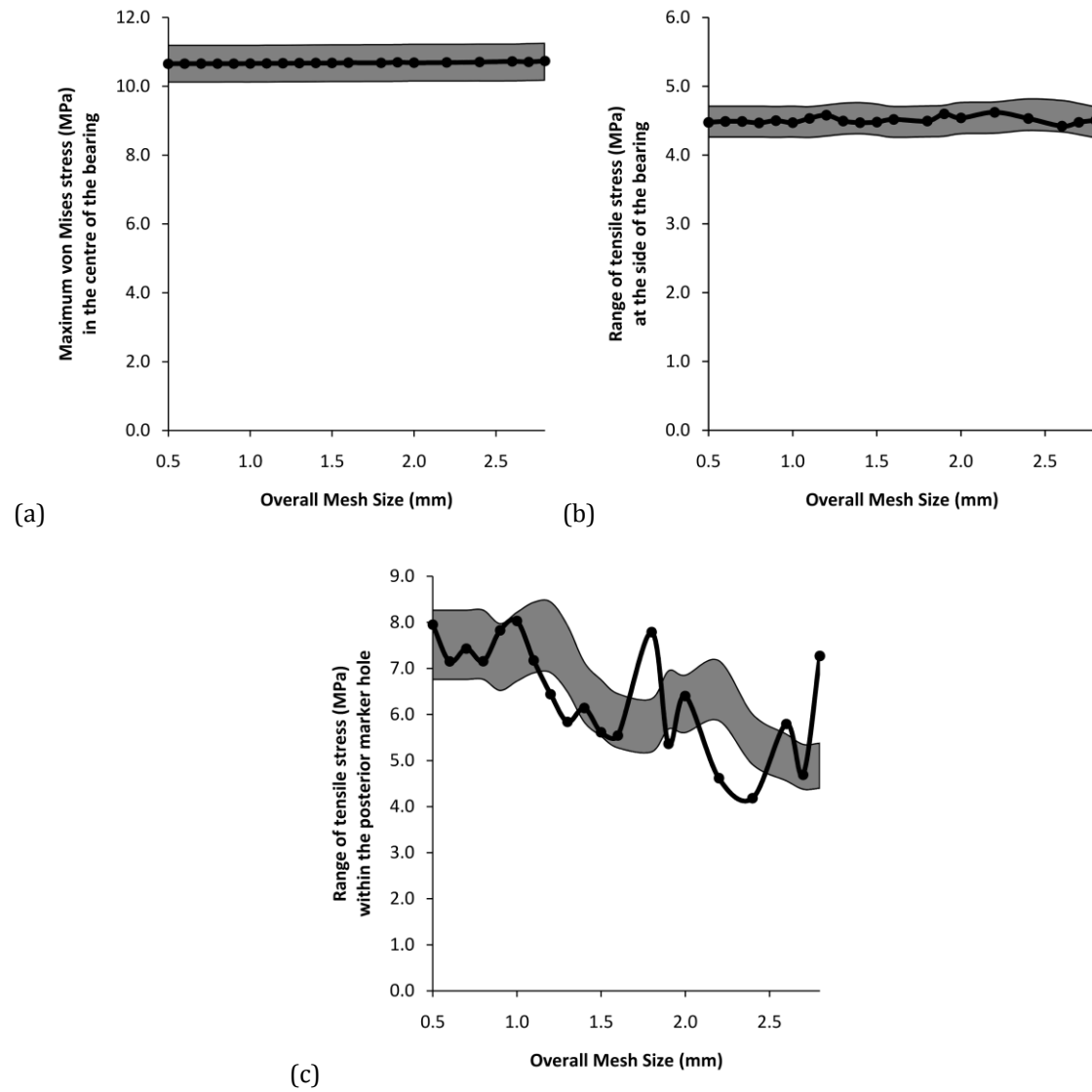


Figure 4. Mesh convergence results for (a) the maximum von Mises stress at the centre of the bearing, (b) the range of tensile stress at the side of the bearing, (c) the range of tensile stress within the posterior marker hole. The area highlighted in grey represents the data within 95% of the next three smaller mesh sizes.

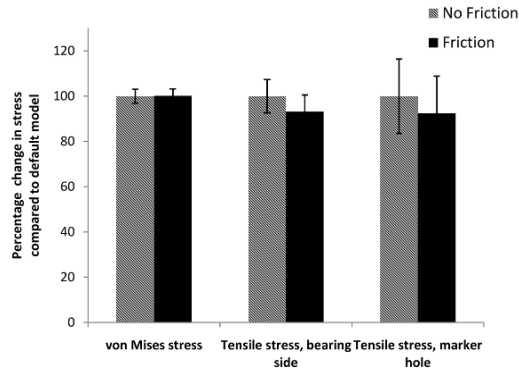


Figure 5. Difference in the von Mises and tensile stresses within the model when friction was included on the tibial side, compared with no friction. No statistical differences were found between the two models.

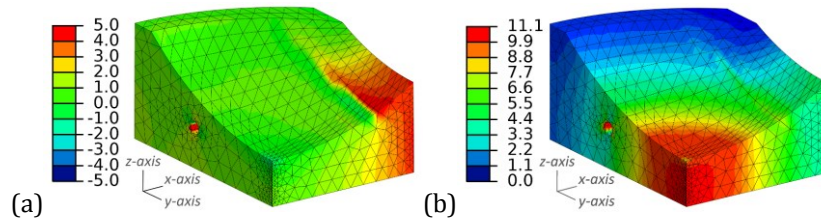


Figure 6. The maximum principal stresses (a) and the von Mises stresses (b) within the posterior half of the bearing at peak load, using default dimensions for the bearing. The mesh density shown is the final mesh decided upon as a result of the mesh convergence test (1 mm). Units are in MPa.

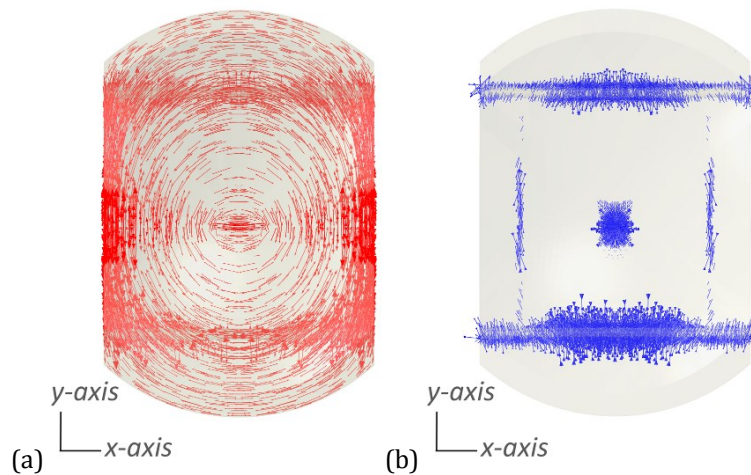


Figure 7. Illustration of the tensile vectors within the bearing of default dimensions. The tensile force magnitude is represented by the arrow size and represents the direction in which the tensile force is acting. The top of the image is the anterior side of the bearing, and the lower is the posterior side.

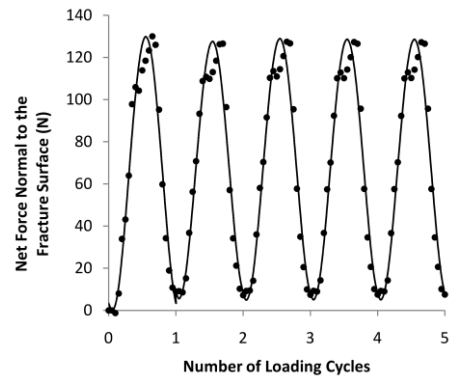


Figure 8. Change in net tensile force normal to the fracture surface over 5 loading cycles for a bearing of default dimensions.

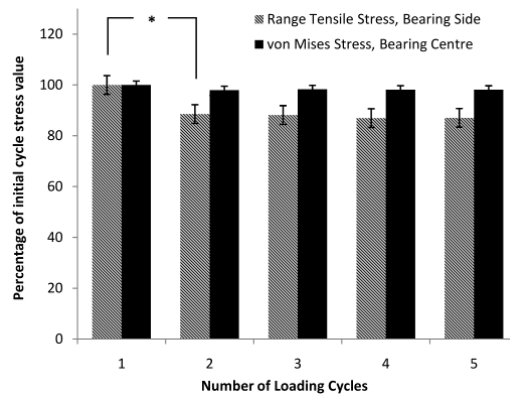


Figure 9. Change in stress with increasing loading cycles for a bearing of default dimensions; data represented as a percentage of the 1<sup>st</sup> cycle. Significance (\*) shown when  $p < 0.05$ .

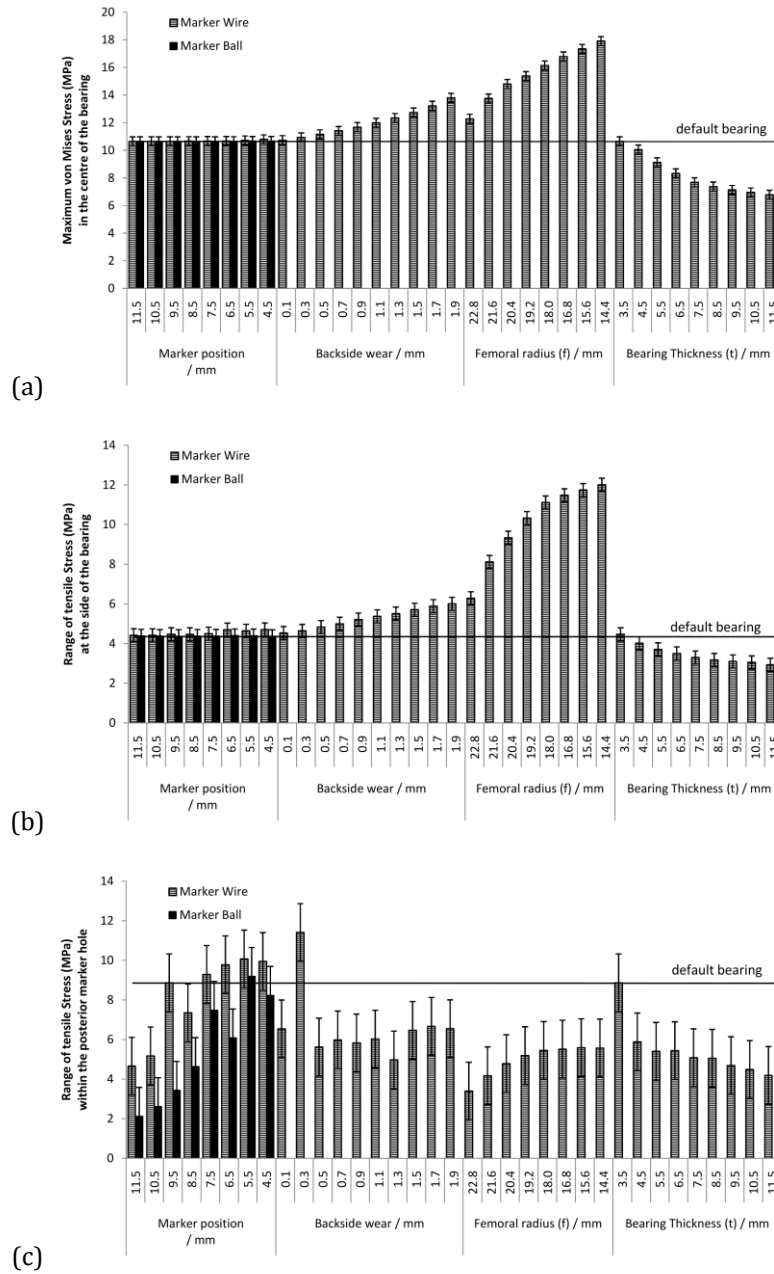


Figure 10. Results summary for the different models illustrating the change in (a) the maximum von Mises stress in the centre of the bearing, (b) the range of tensile stress at the side of the bearing, and (c) the range of tensile stress within the marker hole.

Model	Geometry investigated	Parameter	Values
<b>Model-W</b>	Wire position $y$ -axis	$m_1$	4.5, 5.5, 6.5, 7.5, 8.5, 9.5, 10.5, 11.5
<b>Model-B</b>	Ball position $y$ -axis	$m_1$	4.5, 5.5, 6.5, 7.5, 8.5, 9.5, 10.5, 11.5
<b>Model-W</b>	Backside wear	$m_2$	2.9, 2.7, 2.5, 2.3, 2.1, 1.9, 1.7, 1.5, 1.3, 1.1
		$t$	3.4, 3.2, 3.0, 2.8, 2.6, 2.4, 2.2, 2.0, 1.8, 1.6, 1.4, 1.2
<b>Model-W</b>	Femoral radius	$f$	14.4, 15.6, 16.8, 18.0, 19.2, 20.4, 21.6, 22.8, 24.0
<b>Model-W</b>	Bearing thickness	$t$	3.5, 4.5, 5.5, 6.5, 7.5, 8.5, 9.5, 10.5, 11.5

Table 1. Summary of the different models created, and the values assigned to the parameters.

Overall Mesh Size / mm	Detailed Mesh Size / mm	No. Nodes	No. Elements
<b>0.5</b>	0.15	271921	387984
<b>0.6</b>	0.18	156078	225124
<b>0.7</b>	0.21	108587	157232
<b>0.8</b>	0.24	78936	112287
<b>0.9</b>	0.27	60911	89154
<b>1.0</b>	<b>0.30</b>	<b>39870</b>	<b>59167</b>
<b>1.1</b>	0.33	32388	48455
<b>1.2</b>	0.36	26895	40408
<b>1.3</b>	0.39	21755	32871
<b>1.4</b>	0.42	17044	25912
<b>1.5</b>	0.45	15612	23766
<b>1.6</b>	0.48	12941	19779
<b>1.7</b>	0.51	10668	16477
<b>1.8</b>	0.54	8951	13960
<b>1.9</b>	0.57	8526	13284
<b>2.0</b>	0.60	6858	10764
<b>2.2</b>	0.66	5736	9117
<b>2.4</b>	0.72	4297	6863
<b>2.6</b>	0.78	3674	5947
<b>2.8</b>	0.84	2983	4881

Table 2. Details of the meshes tested for the mesh convergence test.



## References

- 1 **National Joint Registry (NJR).** *National Joint Registry for England and Wales: The 8<sup>th</sup> Annual Report.* Hertfordshire: NJR, 2011.
- 2 **Robine J. M. and Ritchie K.** Healthy life expectancy: evaluation of global indicator of change in population health. *Brit Med J (Clinical research ed).* 1991; 302(6774), 457-60.
- 3 **Pegg E., Pandit H., Gill H. S., et al.** Examination of ten fractured Oxford unicompartmental knee bearings. *J Bone Joint Surg Br.* 2011; 93(12), 1610-6.
- 4 **Argenson J. and O'Connor J.** Polyethylene wear in meniscal knee replacement. A one to nine-year retrieval analysis of the Oxford knee. *J Bone Joint Surg Br.* 1992; 74-B(2), 228-32.
- 5 **Psychoyios V., Crawford R. W., O'Connor J. J. and Murray D. W.** Wear of congruent meniscal bearings in unicompartmental knee arthroplasty: a retrieval study of 16 specimens. *J Bone Joint Surg Br.* 1998; 80(6), 976.
- 6 **Kurtz S. M., van Ooij A., Ross R., et al.** Polyethylene wear and rim fracture in total disc arthroplasty. *Spine J.* 2007; 7(1), 12-21.
- 7 **Wang H.-C., Sung C. and Hamilton J.** Fracture study of ultra high molecular weight polyethylene. *J Mater Sci Lett.* 1998; 17(1), 41-3.
- 8 **Kurtz S. M., Pruitt L., Jewett C. W., Crawford R. P., Crane D. J. and Edidin A. A.** The yielding, plastic flow, and fracture behavior of ultra-high molecular weight polyethylene used in total joint replacements. *Biomaterials.* 1998; 19(21), 1989-2003.
- 9 **Kurtz S. M., Rimnac C. M. and Bartel D. L.** Degradation rate of ultra-high molecular weight polyethylene. *J Orthop Res.* 1997; 15(1), 57-61.
- 10 **Kurtz S. M., Rimnac C. M., Santner T. J. and Bartel D. L.** Exponential model for the tensile true stress-strain behavior of as-irradiated and oxidatively degraded ultra high molecular weight polyethylene. *J Orthop Res.* 1996; 14(5), 755-61.
- 11 **Bergström J. S., Kurtz S. M., Rimnac C. M. and Edidin A. A.** Constitutive modeling of ultra-high molecular weight polyethylene under large-deformation and cyclic loading conditions. *Biomaterials.* 2002; 23(11), 2329-43.
- 12 **Georgette F. S.** *Effect of hot isostatic pressing on the mechanical and corrosion properties of a cast, porous-coated Co-Cr-Mo alloy.* Philadelphia, PA, USA: American Society for Testing and Materials, 1987, p.16.
- 13 **Harrysson O. L. A., Cansizoglu O., Marcellin-Little D. J., Cormier D. R. and West li H. A.** Direct metal fabrication of titanium implants with tailored materials and mechanical properties using electron beam melting technology. *Mat Sci Eng C.* 2008; 28(3), 366-73.
- 14 **Bale M. D. and May A. V.** Processing of ores to produce tantalum and lithium. *Minerals Engineering.* 1989; 2(3), 299-320.
- 15 **Crockett R., Roba M., Naka M., et al.** Friction, lubrication, and polymer transfer between UHMWPE and CoCrMo hip-implant materials: A fluorescence microscopy study. *J Biomed Mat Res A.* 2009; 89A(4), 1011-8.
- 16 **Morrison J. B.** The mechanics of the knee joint in relation to normal walking. *J Biomech.* 1970; 3(1), 51-61.
- 17 **Olovsson L., Simonsson K. and Unosson M.** Selective mass scaling for explicit finite element analyses. *Int J Numer Meth Eng.* 2005; 63(10), 1436-45.
- 18 **Dar F. H., Meakin J. R. and Aspden R. M.** Statistical methods in finite element analysis. *J Biomech.* 2002; 35(9), 1155-61.
- 19 **Prior A. M.** Applications of implicit and explicit finite element techniques to metal forming. *Journal of Materials Processing Technology.* 1994; 45(1-4), 649-56.

- 20 **Brimacombe J. M., Wilson D. R., Hodgson A. J., Ho K. C. T. and Anglin C.** Effect of Calibration Method on Tekscan Sensor Accuracy. *Journal of Biomechanical Engineering*. 2009; 131(3), 034503.
- 21 **Schijve J.** Fatigue of structures and materials in the 20th century and the state of the art. *Int J Fatigue*. 2003; 25(8), 679-702.
- 22 **Pruitt L. A.** Deformation, yielding, fracture and fatigue behavior of conventional and highly cross-linked ultra high molecular weight polyethylene. *Biomaterials*. 2005; 26(8), 905-15.
- 23 **Pascaud R. S., Evans W. T., McCullagh P. J. J. and FitzPatrick D. P.** Influence of gamma-irradiation sterilization and temperature on the fracture toughness of ultra-high-molecular-weight polyethylene. *Biomaterials*. 1997; 18(10), 727-35.
- 24 **Plumbridge W. J. and Ryder D. A.** The influence of specimen geometry on the mode of fatigue crack growth in aluminium. *Acta Metallurgica*. 1969; 17(12), 1449-52.
- 25 **Plumbridge W. J.** Review: Fatigue-crack propagation in metallic and polymeric materials. *J Mat Sci*. 1972; 7(8), 939-62.
- 26 **Estupiñán J. A., Bartel D. L. and Wright T. M.** Residual stresses in ultra-high molecular weight polyethylene loaded cyclically by a rigid moving indenter in nonconforming geometries. *J Orthop Res*. 1998; 16(1), 80-8.
- 27 **Krzypow D. J. and Rinnac C. M.** Cyclic steady state stress-strain behavior of UHMW polyethylene. *Biomaterials*. 2000; 21(20), 2081-7.
- 28 **Goodfellow J., O'Connor J. J., Dodd C. and Murray D. W.** *Unicompartmental arthroplasty with the Oxford knee*. Oxford: Oxford University Press, 2006.
- 29 **Bell C. J., Walker P. S., Abeysondera M. R., Simmons J. M. H., King P. M. and Blunn G. W.** Effect of oxidation on delamination of ultrahigh-molecular-weight polyethylene tibial components. *J Arthroplasty*. 1998; 13(3), 280-90.
- 30 **Bergström J. S., Rinnac C. M. and Kurtz S. M.** Prediction of multiaxial mechanical behavior for conventional and highly crosslinked UHMWPE using a hybrid constitutive model. *Biomaterials*. 2003; 24(8), 1365-80.
- 31 **Currier B. H., Currier J. H., Mayor M. B., Lyford K. A., Van Citters D. W. and Collier J. P.** In vivo oxidation of  $\gamma$ -barrier-sterilized ultra-high-molecular-weight polyethylene bearings. *J Arthroplasty*. 2007; 22(5), 721-31.
- 32 **Medel F. J., Rinnac C. M. and Kurtz S. M.** On the assessment of oxidative and microstructural changes after in vivo degradation of historical UHMWPE knee components by means of vibrational spectroscopies and nanoindentation. *J Biomed Mat Res A*. 2009; 89A(2), 530-8.
- 33 **Kendrick B., Simpson D., Gill H., et al.** Unicompartmental knee replacement as a definitive implant: 20 year in-vivo wear data. *J Bone Joint Surg Br*. 2011; 93-B(SUPP II), 208.